Article

Cooling Performance Characteristics of 20 Ah Lithium-Ion Pouch Cell with Cold Plates along Both Surfaces

Mahesh Suresh Patil [1] [ID], **Satyam Panchal [2], Namwon Kim [3] and Moo-Yeon Lee [1],*** [ID]

[1] Department of Mechanical Engineering, Dong-A University, 37 Nakdong-Daero 550, Saha-gu, Busan 604-714, Korea; msp692@gmail.com

[2] Mechanical and Mechatronic Engineering Department, University of Waterloo, 200 University Avenue West, Waterloo, ON N2L 3G1, Canada; satyam.panchal@uwaterloo.ca

[3] Ingram School of Engineering, Texas State University, San Marcos, TX 78666, USA; namwonkim@txstate.edu

* Correspondence: mylee@dau.ac.kr; Tel.: +82-51-200-7642

check for updates

Abstract: Temperature control of the lithium-ion pouch cells is crucial for smooth operation, longevity and enhanced safety in the battery-operated electric vehicles. Investigating the thermal behavior of lithium-ion pouch cells and optimizing the cooling performance are required to accomplish better performance, long life, and enhanced safety. In the present study, the cooling performance characteristics of 20 Ah lithium-ion pouch cell with cold plates along both surfaces are investigated by varying the inlet coolant mass flow rates and the inlet coolant temperatures. The inlet coolant mass flow rate is varied from 0.000833 kg/s to 0.003333 kg/s, and the inlet coolant temperature is varied from 5 °C to 35 °C. In addition, the effects of the cold plate geometry parameter on cooling performance of 20 Ah lithium-ion pouch cell are studied by varying the number of the channels from 4 to 10. The maximum temperature and difference between the maximum and the minimum temperatures are considered as important criteria for cooling performance evaluation of the 20 Ah lithium-ion pouch cell with cold plates along both surfaces. The cooling energy efficiency parameter (β) and the pressure drop for 20 Ah lithium-ion pouch cell with cold plates along both surfaces are also reported. The study shows that enhanced cooling energy efficiency is accompanied with low inlet coolant temperature, low inlet coolant mass flow rate, and a high number of the cooling channels. As a result, the temperature distribution, the pressure drop, and the cooling energy efficiency parameter (β) of the 20 Ah lithium-ion pouch cell with cold plates along both surfaces are provided, and could be applied for optimizing the cooling performances of the thermal management system for lithium-ion batteries in electric vehicles.

Keywords: cold plate; cooling; electric vehicle; lithium-ion; performance

1. Introduction

The exponential increase in energy demand, concerns over environmental degradation due to the effects of greenhouse gases, and the depletion of fossil fuels have resulted in stricter emission laws, making alternative, renewable energy sources a sustainable and promising option. Fossil fuel-based transport and associated sectors accounted for about 30–35% in many developed countries [1]. Recently, batteries used in electric vehicles (EVs) have gathered reasonable importance as a possible means to reduce fossil fuel dependence. In EVs, the battery serves as a power source for driving the vehicle, and can be recharged before use, as compared to internal combustion engine (ICE) operated automotives, where power is derived from the combustion of fossil fuel.

A stack of battery packs is the primary power source in many modern EVs. A single battery pack is composed of many modules; each module is composed of many battery cells, making the single cell the fundamental unit of the power source for EVs. As a result, the overall performance, range, and operation of EVs are affected by the performance of the battery pack, module, and individual single cell. Lithium-ion batteries have high specific power and specific energy densities, lower discharge rates when not in use leading to better shelf life, relatively longer charge-discharge life cycles, and faster charging capabilities, which makes them favorable as the power source to drive EVs [2–4]. Zubi et al. conducted a comprehensive review about the current state of lithium-ion batteries, and determined that lithium-ion batteries have the capability of developing as an essential segment of future energy needs, including in the automotive sector [5]. However, the degradation of lithium-ion batteries' capabilities in terms of capacity fade, power fade, and self-discharge at extreme temperatures indicates temperature influence; a temperature range of 25 °C to 40 °C could be considered as favorable for optimal operation [6]. For lower temperatures, the reduction in power is attributed to higher internal resistance, and for higher temperatures, the reduction in lifespan is attributed to thermal deterioration. In the absence of an efficient cooling system, the battery temperature escalates due to heat accumulation, and could lead to thermal runaway damaging whole battery power source [7,8]. In thermal runaway, a large number of chain chemical reactions occur continuously, leading to a short circuit, with the possibility of fire. Safety in the battery-operated vehicles is one of the main impediments for comprehensive usage of batteries in the vehicles, making the thermal management of batteries a very important aspect for the advancement of EVs [9].

The cooling strategy employed in the battery thermal management system needs to maintain maximum temperature, average temperature, and temperature evenness in the battery pack, as well as in each cell in the specified working temperature range, for better performance [6]. A variety of cooling strategies are being investigated for lithium-ion batteries, with different coolants such as air, mineral oil, heat pipes, water, and phase change material (PCM). Among the various cooling methods and coolants, water-based cooling systems have generated much attention, as water has excellent thermal properties as a coolant [10]. Air-based cooling strategies have the advantage of a simplified arrangement and little maintenance, but suffer from limitations in maximum heat removal capacity. In addition, the noise issue due to the high fan speed makes this solution undesirable [11]. Integrating PCM into the cooling system has shown the advantage of even temperature distribution; however, the low cooling efficiency issue needs to be resolved [12]. PCM-based cooling could be a promising option provided that the thermal conductivity of PCM is improved [13]. Mineral oil, due to its dielectric behavior, could be used for direct cooling with better efficiency, but feasibility for practical usage needs to be tested [14,15]. Comparing a variety of cooling strategies, water-based cooling systems provide excellent cooling, and have the advantage of less volume requirement due to compactness. Panchal et al. [16] conducted an experimental and numerical study on the thermal behavior of prismatic lithium-ion battery cells by employing a mini-channel cold plate, and suggested that CFD simulations could be used in the design and optimization of battery cooling systems. In a supplement to the above discussion, major automotive manufacturing companies such Tesla, Hyundai, General Motors etc. are using water-based cooling methods for temperature control of the lithium-ion pouch cells in EVs.

One of the methods to enhance the travel range of EVs is to design lithium-ion batteries with higher energy densities which can provide more power per unit weight [17]. Throughout the last decade, the enhancement in the energy density of lithium-ion batteries has resulted in a corresponding increase in EV travel range. However, high energy density lithium-ion batteries have the disadvantage of high heat generation. Therefore, effective and compact cooling is necessary for safe operation and longevity [18,19]. The optimization of existing cooling methods is one of the effective ways to enhance the cooling capability.

In the present study, the cooling performance characteristics of lithium-ion pouch cells with cold plates on both surfaces are numerically investigated. The input parameters are varied by changing the inlet coolant mass flow rate and temperature for 1C and 2C discharge rates. The validation of

numerical analysis is conducted by comparing with experimental results provided by Panchal et al. [20]. Maximum temperature, temperature difference, pressure drop, and cooling energy efficiency parameters are studied as performance evaluating parameters. In addition, the effects of a different number of channels on the cooling performance of a 20 Ah lithium-ion pouch cell are studied.

2. Numerical Analysis

The numerical analysis was composed of geometrical modeling, mesh generation, mesh independency test, initial and boundary conditions, and solving governing equations. The mesh independency test demonstrated that the numerical analysis outcome is insensitive to the number of elements in the mesh. Considering the computational cost as well as the mesh sensitivity, the particular mesh for conducting a numerical study is chosen. The initial and boundary conditions are employed by considering the experimental analysis, and validation is conducted by comparing the numerical and experimental results [20]. The numerical study provides insight into enhancing the cooling performance and the design improvement at minimal cost, and is useful for the advancement of thermal management of lithium-ion batteries in the EVs.

2.1. Physical Model

The visual specifics of the geometrical model, the schematic, and the meshing of 20 Ah lithium-ion pouch cell with cold plates along both surfaces is shown in the Figure 1. The computer-aided design (CAD) model of 20 Ah lithium-ion pouch cell with cold plates along both surfaces was developed based on the dimensions of the experimental study, as shown in the Figure 1a. The overall size of the numerical domain in the present study is 205 mm × 157 mm × 10.4 mm. It consists of a 20 Ah lithium-ion pouch cell and cold plates attached to a lateral surface of the battery. The geometry specifications are presented in the Table 1. The size of the cold plate used in the analysis is 205 mm × 157 mm × 1.7 mm. The 20 Ah lithium-ion pouch cell properties are shown in Table 2. The schematic of the model is provided in Figure 1b, with details of the inlet and outlet for the coolant. Large 20 Ah lithium-ion pouch cells are used in the electric vehicles (EV) and hybrid electric vehicles (HEV) as a power source, and therefore, were considered in the present study. To assess the influence of geometry modification on the cooling performance of the 20 Ah lithium-ion pouch cell, four different types of cold plates are considered. Figure 2 shows the cold plates with the number of cooling channels varying from 4 to 10.
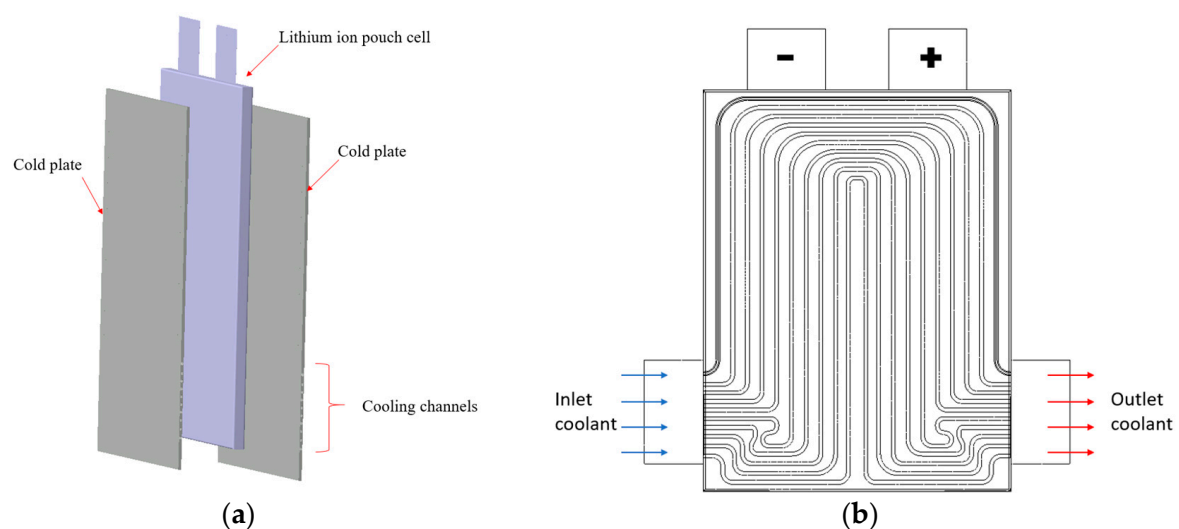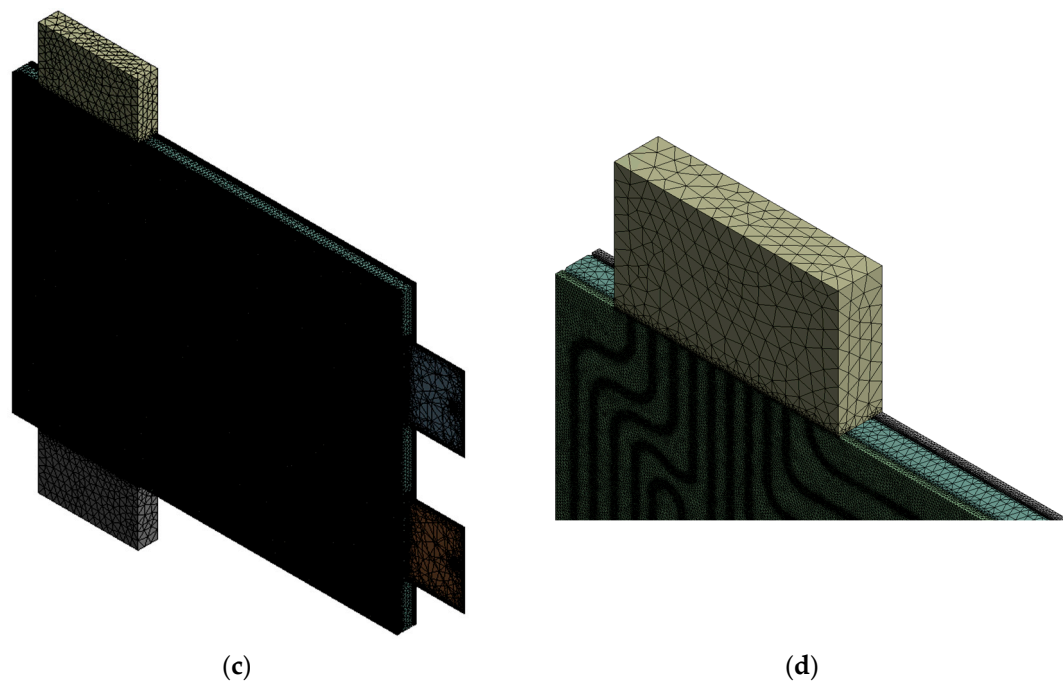

(a)

(b)

Figure 1. *Cont.*

(**c**)　　　　　　　　　　　　　　　　　　　　　　　　(**d**)

Figure 1. Numerical model for the 20 Ah lithium-ion pouch cell with cold plates along both surfaces (**a**) Geometry (**b**) Schematic (**c**) Meshing-full domain (**b**) Meshing-section.

Table 1. Geometry details.

Parameter	Value
Overall size (mm^3)	$205 \times 157 \times 10.4$
Battery size (mm^3)	$205 \times 157 \times 7$
Cold plate size (mm^3)	$205 \times 157 \times 1.7$
Number of cooling channels	4, 6, 8, 10

Table 2. 20Ah Li-ion pouch cell specifications [20].

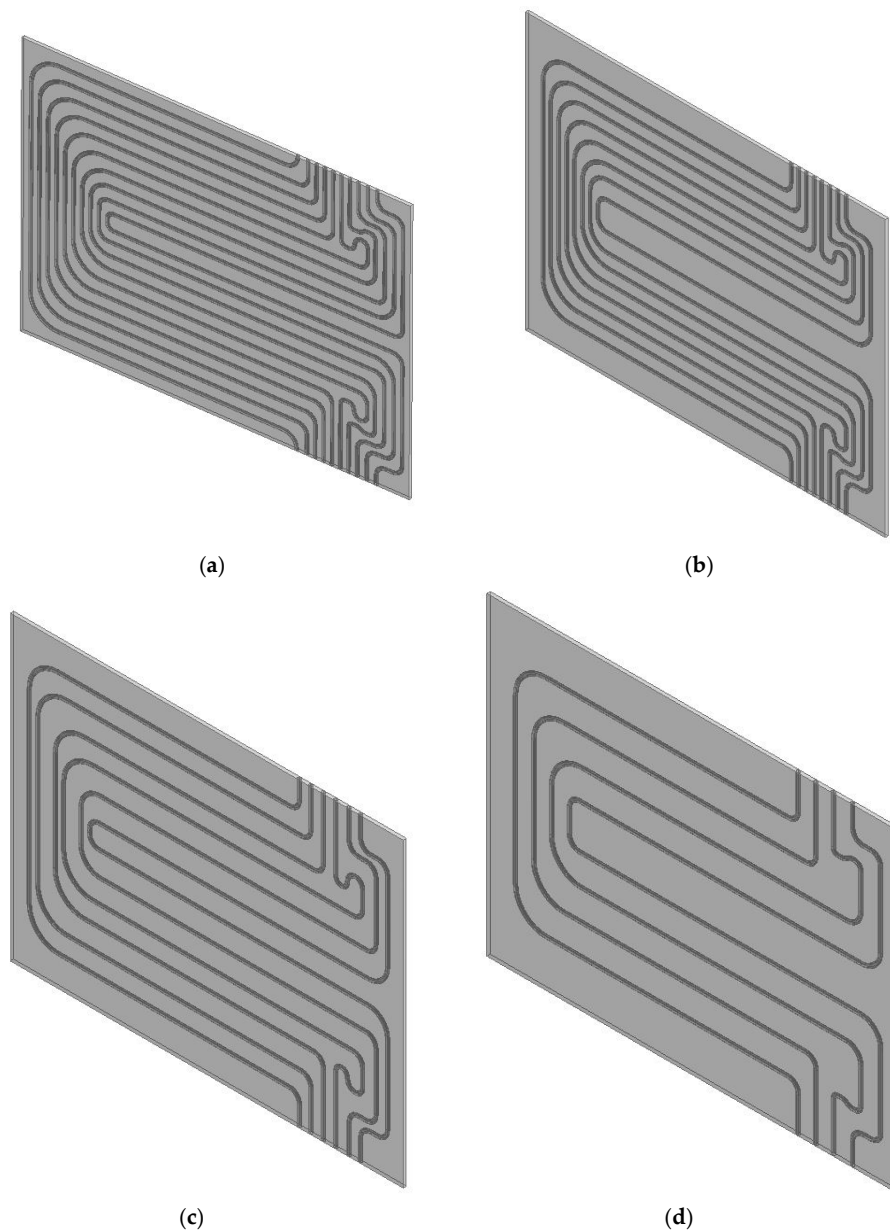| Parameter	Value
Cathode material	LiFePO$_4$
Anode material	Graphite
Electrolyte	Carbonate based
Nominal capacity (Ah)	20.0
Nominal Energy (Wh)	65
Energy density (Wh/L)	247
Mass (g)	496
Specific power (W/kg)	2400
Specific energy (Wh·kg)	131
Volume (L)	0.263
Density (kg/m^3)	1940
Thermal conductivity (W/m·K)	18.2
Specific heat capacity (J/kg·K)	1000

Figure 2. Cold plates with the different number cooling channels for 20 Ah lithium-ion pouch cell (**a**) 10; (**b**) 8; (**c**) 6; (**d**) 4.

2.2. Numerical Method

The present study is treated as turbulent fluid flow with heat transfer based on the Reynolds number, 8.7×10^3, for circular pipes obtained in the experiment [20]. ANSYS Meshing (ANSYS 18.0, Ansys Inc., Canonsburg, PA, USA) is used to resolve the simulation domain into finer elements. The governing equations, including Navier-stokes equations and turbulence equations, are solved using the commercial code ANSYS CFX 18.0 solver [21], and reliable results are obtained by setting appropriate convergence criteria. The details of continuity, momentum conservation, and energy conservation are given from Equations (1)–(3). CFD technique provides comprehensive results extending over the complete numerical domain, as compared to experimental study, where data is obtained at specific points. As temperature distribution is of interest in the present study, the energy equation is also solved.

$$\nabla * \overline{V} = 0 \tag{1}$$

$$\rho\left[\frac{\partial\overline{V}}{\partial t} + (\vec{V}\cdot\nabla\overline{V})\right] = -\nabla\overline{p} + (\mu\nabla^2\overline{V} - \lambda) \tag{2}$$

$$\frac{\partial\rho T}{\partial t} + \nabla * [\rho\vec{V}T] = \nabla * \left[\left(\frac{\mu}{\text{Pr}} + \frac{\mu_t}{\text{Pr}_t}\right)\nabla T\right] \tag{3}$$

For all cases, the k-ε turbulent model with a turbulent intensity of 5% is considered for turbulence modeling based on Reynolds number and low-medium level turbulence. The equations for turbulent kinetic energy and eddy viscosity are given in Equations (4) and (5).

$$\frac{\partial\rho k}{\partial t} + \nabla * [\rho\vec{V}k] = \nabla * \left[\left(\mu + \frac{\mu_t}{\sigma_k}\right)\nabla k\right] + G_k + G_b - \rho\varepsilon - Y_M + S_k \tag{4}$$

$$\frac{\partial\rho\varepsilon}{\partial t} + \nabla * [\rho\vec{V}\varepsilon] = \nabla * \left[\left(\mu + \frac{\mu_t}{\varepsilon_k}\right)\nabla\varepsilon\right] + C_1\frac{\varepsilon}{k}(G_k + C_3G_b) - C_2\rho\frac{\varepsilon^2}{k} + S_\varepsilon \tag{5}$$

In Equations (4) and (5), C_1, C_2, and C_3 are provided as the model constants, and σ_k and σ_ε are the corresponding turbulent Prandtl numbers for k and ε. Sk and $S\varepsilon$ represent user-defined source terms. The eddy viscosity is computed by Equation (6):

$$\mu_t = C_\mu\rho\frac{k^2}{\varepsilon} \tag{6}$$

Water is considered as the coolant in the current numerical analysis, and the coolant flow is assumed to be incompressible. The thermophysical properties including thermal conductivity, specific heat, and viscosity of the coolant are considered independent of temperature. The temperature of the battery, the cold plate, and the coolant changed throughout the numerical domain according to the location.

Table 3 shows the boundary conditions employed for setting up the numerical simulation. Table 4 shows the heat generation rates for the different discharge rates and different inlet coolant temperatures with water as coolant, provided by the experimental study [20].

Table 3. Boundary conditions.

Parameter	Value
Coolant	Water
Inlet coolant temperature (°C)	5, 15, 25, 35
Inlet coolant mass flow rate (kg/s)	0.000833, 0.001667, 0.002500, 0.003333
Current discharge rate (C)	1, 2
Turbulence model	k-ε
Turbulent intensity (%)	5
Turbulent viscosity ratio	10

Table 4. Experimental results for the maximum heat generation rate at 1C, 2C discharge rates and the different boundary conditions [20].

Cooling Types	Inlet Coolant Temperatures (°C)	Maximum Heat Generation Rates (W)	
Coolant	Water	1C	2C
	5	24.0	50.4
Active (U-turn cold plate)	15	22.5	44.2
	25	19.4	36.9
	35	12.5	29.5

The mesh generation of the lithium-ion pouch cell with cold plates on both surfaces is shown in the Figure 1c,d. After meshing, 9,407,382 elements are generated with 1,662,537 nodes. The minimum and the maximum orthogonal qualities of 0.1731 and 0.998 are reported to be within the acceptable quality. A total of five mesh models are employed to investigate the mesh independency test of the numerical study. Table 5 shows the details of the mesh with the number of elements. Figure 3 shows that as the element numbers increased from 4,612,864 to 10,647,327, and that the average outlet coolant temperature and the average pressure drop are converged within 0.025% and 0.033% after the element numbers of 9,407,382. As a result, mesh with the element number of 9,407,382 is selected for the numerical analysis, considering accuracy as well as computational cost.

Table 5. Mesh details.

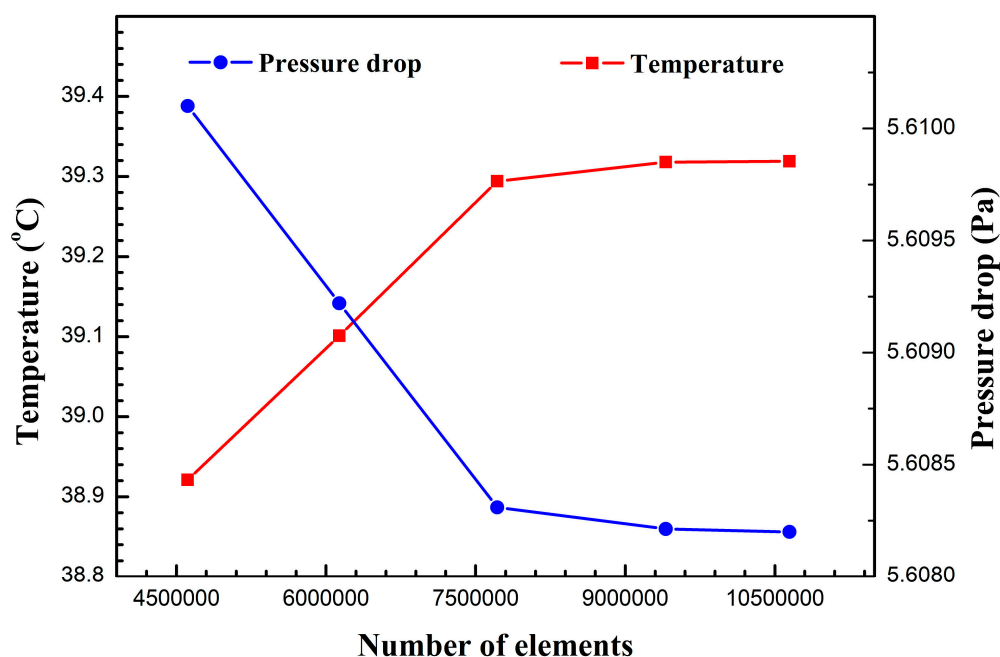| Mesh Type	Number of Elements
Type 1	4,612,864
Type 2	6,134,164
Type 3	7,716,948
Type 4	9,407,382
Type 5	10,647,326

Figure 3. Mesh independency test.

2.3. Data Reduction

The effectiveness of the 20 Ah lithium-ion pouch cell with cold plates along both surfaces is evaluated in terms of the key parameter of β. The parameter β is defined as the cooling energy efficiency, and is employed to evaluate the cooling effectiveness. The parameter β could be determined using the following equations:

$$\beta = \frac{\text{Heat taken away by liquid coolant from lithium} - \text{ion pouch cell}}{\text{Power consumption for supplying liquid coolant}} \tag{7}$$

To specifically compare the relationship between heat removal rate and pumping power for various geometry arrangements with different number of cooling channels, in Equation (7), in the

denominator, the power needed to cool the used coolant down to inlet temperature is neglected. From Equation (7) it can be understood that a higher beta value corresponds to effective cooling. The increase in the mass flow rate affects numerator and denominator simultaneously. The heat transfer rate from the liquid coolant is calculated by Equation (8), and the power consumption for supplying liquid coolant through channels is calculated by Equation (9).

$$Q = \dot{m} \times c_p \times \Delta T \tag{8}$$

$$P = P_{drop} \times Q_v \tag{9}$$

The cooling performance is dependent on the available area for heat transfer. In the present study, the effect of available surface area on cooling performance can be evaluated by a non-dimensional parameter α. The parameter α is called as surface area coverage ratio, and is defined as the ratio of surface area of cooling channels and the lateral surface area of cell. Here, the total surface area of all the circular channels and only the side surface of the battery are considered, i.e., where predominantly generated heat is removed by the coolant. Table 6 shows the details of surface area coverage ratio in the present study.

$$\alpha = \frac{\text{Surface area of cooling channels}}{\text{Lateral surface area of battery}} \tag{10}$$

Table 6. Surface area coverage ratio.

Number of Channels	Side Surface Area of Single Cell (mm^2)	Surface Area of all the Channels for One Side of the Battery (mm^2)	Surface Area Coverage Ratio
4	31,465	9387.9	0.298
6	31,465	14,188.6	0.450
8	31,465	18,873.5	0.599
10	31,465	23,606.8	0.750

3. Results and Discussion

Literature exists for the water jacket cooling [22] and mini channel cold plate cooling [23], but detailed analysis of U-turn cold plates with varying the inlet coolant mass flow rates, the inlet coolant temperatures and the number of cooling channels on both side surfaces of the lithium-ion pouch cell are not reported. Therefore, the cooling performance characteristics of the 20 Ah lithium-ion pouch cell with cold plates along both surfaces are numerically investigated with variations of the inlet coolant mass flow rate and the inlet coolant temperature for 1C and 2C discharge rates. The temperature distribution, the pressure drop, and the cooling energy efficiency parameter (β) are considered as the performance parameters. In addition, variations in the cold plate geometry are considered with different numbers of the cooling channels, and the subsequent effect on the cooling performance is investigated.

3.1. Validation

To validate the accuracy of the numerical simulation results with the experimental results, the maximum temperature of 20 Ah lithium-ion pouch cell with varying the inlet coolant temperature is considered. A comparison of the experimental and the numerical simulation is carried out by employing similar geometries, dimensions, and boundary conditions. Figure 4 shows the comparison of the numerical results with the experimental results provided by Panchal et al. [20]. The comparison showed good agreement within ±13% of the existed data; thus, validation is confirmed.
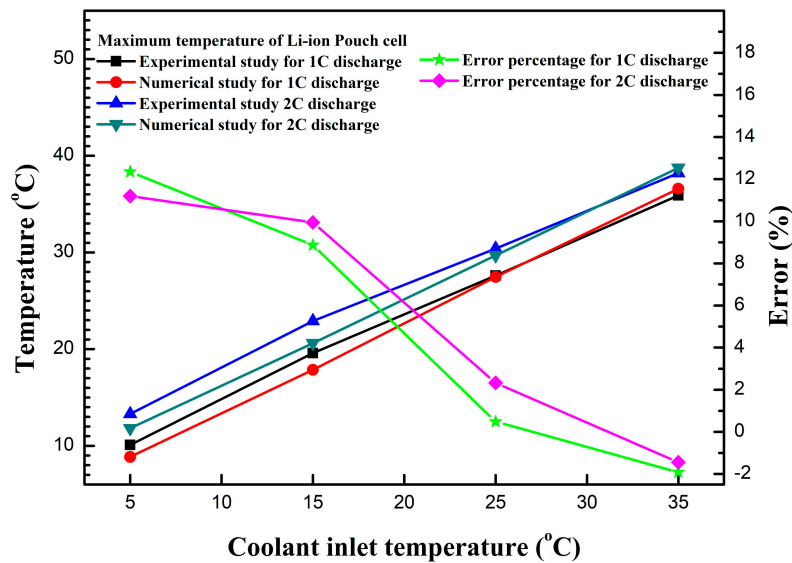
Figure 4. Validation [20].

3.2. Temperature Distribution

Internal resistance leading to ohmic heating, and electrochemical reactions leading to entropy change, contribute to heat generation during the battery cell operation. The generated heat could increase the battery temperature owing to heat accumulation. The increase in temperature affects the battery capacity as well as its resistance. This is significant for the advancement of EVs, as vehicle driving range is dependent on battery cell and operating temperature. The maximum temperature and the temperature non-uniformity in the battery during the operation are two critical criteria for quantifying the performance of the battery cooling system. The temperature non-uniformity in the battery is an indicator of uneven temperature distribution, and is defined as the difference between the maximum and minimum temperature of the battery. Figure 5 shows the maximum temperature distribution for the 20 Ah lithium-ion pouch cell with surface area coverage ratio (α) parameter of 0.750. Figure 5a,b show the maximum temperature distribution for the 20 Ah lithium-ion pouch cell for 1C and 2C discharge rates, respectively. For both 1C and 2C discharge rates, the maximum temperature decreased with an increase of the inlet coolant mass flow rate varying from 0.000833 kg/s to 0.003333 kg/s, with surface area coverage ratio (α) parameter of 0.750.

Figure 5a shows that the maximum temperature increased by 392.3% as the inlet coolant temperature increased from 5 °C to 35 °C at the inlet coolant mass flow rate of 0.003333 kg/s. As shown in the Figure 5a, the maximum temperature decreased by 8.5% as the inlet coolant mass flow rate increased from 0.000833 kg/s to 0.003333 kg/s at an inlet coolant temperature of 35 °C and the maximum temperature increased by 80.6% as the inlet coolant mass flow rate increased from 0.000833 kg/s to 0.003333 kg/s at an inlet coolant temperature of 5 °C. Figure 5b shows that the maximum temperature increased by 280.7% as the inlet coolant temperature increased from 5 °C to 35 °C at the inlet coolant mass flow rate of 0.003333 kg/s. As shown in the Figure 5b, the maximum temperature increased by 19.2% as the inlet coolant mass flow rate increased from 0.000833 kg/s to 0.003333 kg/s at an inlet coolant temperature of 35 °C. The maximum temperature increased by 125.2% as the inlet coolant mass flow rate increased from 0.000833 kg/s to 0.003333 kg/s at an inlet coolant temperature of 5 °C. This indicates that, for both 1C and 2C discharge rates, the higher inlet coolant mass flow rate and the lower inlet coolant temperature provides the lower maximum temperature in the lithium-ion pouch cell with cold plates along both surfaces. As shown in Figure 5a,b, when the inlet coolant mass flow rates varied from 0.001667 kg/s to 0.003333 kg/s, the reduction scale of the maximum temperature is lower than those of the inlet coolant mass flow rates varying from 0.000833 kg/s to 0.001667 kg/s for the different inlet coolant temperatures. Comparing with Figure 5a

and Figure 5b, the maximum temperatures show similar trends; however, the maximum temperatures for 2C discharge rate are higher than those for 1C discharge rate. As shown in the Figure 5b, the highest maximum temperature is maintained below 45 °C for all cases, except for the inlet coolant temperature of 35 °C and the inlet coolant mass flow rate of 0.000833 kg/s. Except for this one case, the maximum temperature is maintained below 40 °C, which, as suggested by many researchers, yields optimum performance [6]. The variation in the inlet coolant temperatures has a significant effect on the maximum temperatures of the lithium-ion pouch cell as compared with variations in an inlet coolant mass flow rate. Therefore, it can be concluded that for providing optimum operating temperature in the ranges from 25 °C to 40 °C for the lithium-ion pouch cell for 1C and 2C discharge rates with cold plates along both surfaces, inlet coolant temperatures of 15 °C and 25 °C are suggested.
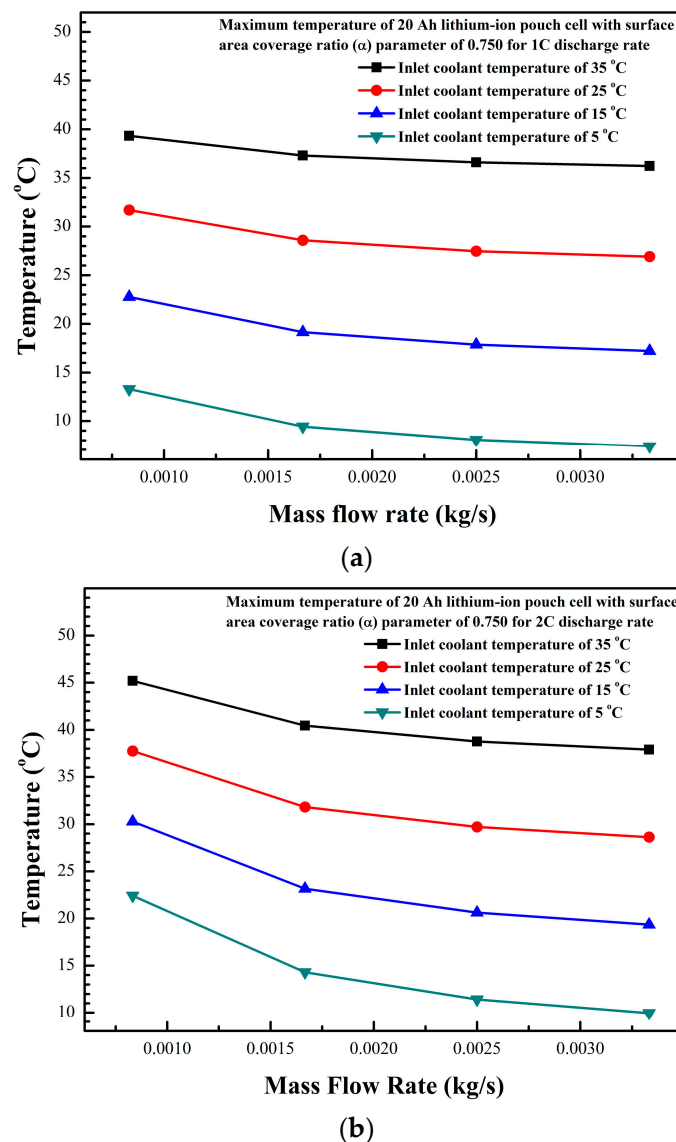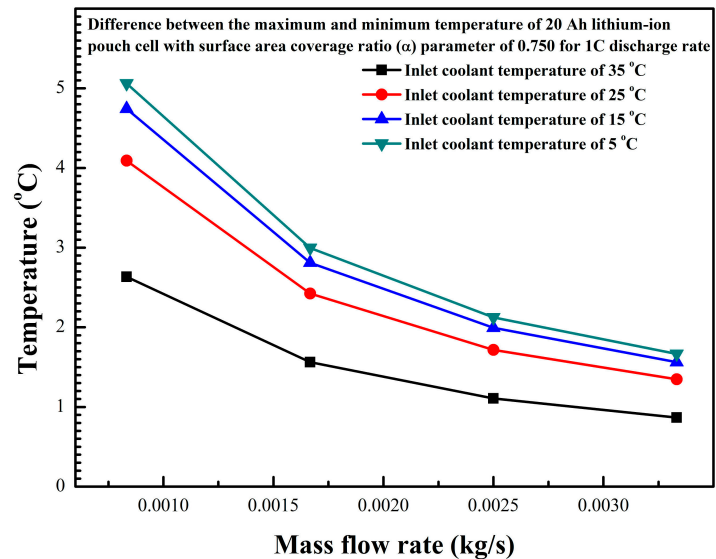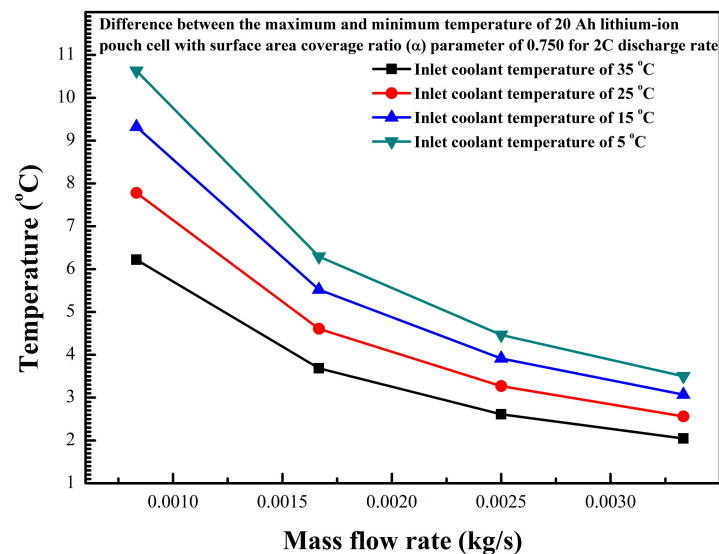

(**a**)

(**b**)

Figure 5. Maximum temperature of 20 Ah lithium-ion pouch cell with surface area coverage ratio (α) parameter of 0.750: (**a**) 1C; (**b**) 2C.

Temperature non-uniformity may cause capacity reduction and hikes in resistance, which may ultimately speed up non-uniform aging of the lithium-ion pouch cell [24]. Figure 6 shows the difference between the maximum and the minimum temperature of 20 Ah lithium-ion pouch cell with surface area coverage ratio (α) parameter of 0.750. Figure 6a,b show the difference between the maximum and the minimum of 20 Ah lithium-ion pouch cell for 1C and 2C discharge

rates, respectively. For both 1C and 2C discharge rates, the difference between the maximum and the minimum temperature decreased with increase of the inlet coolant mass flow rate varied from 0.000833 kg/s to 0.003333 kg/s for surface area coverage ratio (α) parameter of 0.750.

(**a**)

(**b**)

Figure 6. Difference between the maximum and minimum temperature of the 20 Ah lithium-ion pouch cell with surface area coverage ratio (α) parameter of 0.750: (**a**) 1C; (**b**) 2C.

For the low inlet coolant mass flow rate, the difference between the maximum and the minimum temperature significantly decreased with an increase of the inlet coolant temperature. However, for the higher inlet coolant mass flow rates, the difference between the maximum and minimum temperatures is changed slightly with an increase of the inlet coolant temperature. This indicates that, for both 1C and 2C discharge rates, the higher inlet coolant mass flow rate and the higher inlet coolant temperature provides the better temperature uniformity considering the difference between the maximum and the minimum temperature in 20 Ah lithium-ion pouch cell with cold plates along both surfaces. As shown in Figure 6a,b, for the inlet coolant mass flow rates varying from 0.001667 kg/s to 0.003333 kg/s, the reduction scale of the difference between the maximum and the minimum

temperature is lower than those of the inlet coolant mass flow rates varying from 0.000833 kg/s to 0.001667 kg/s for the different inlet coolant temperatures. Comparing with Figure 6a and Figure 6b, the difference between the maximum and the minimum temperatures are close for 1C discharge rate for the inlet coolant temperatures of 5 °C and 15 °C, when the inlet coolant mass flow rate coolant varied from 0.000833 kg/s to 0.003333 kg/s. As shown in the Figure 6b, the highest difference between the maximum and the minimum temperature is maintained below 5 °C for the inlet coolant mass flow rates of 0.002500 kg/s and 0.003333 kg/s. Therefore, it can be concluded that for providing optimum operating difference between the maximum and the minimum temperature below 5 °C for the 20 Ah lithium-ion pouch cell for 1C and 2C discharge rates with cold plates along both surfaces, the inlet coolant mass flow rates of 0.002500 kg/s and 0.003333 kg/s are suggested.

3.3. Pressure Drop

Figure 7 shows the pressure drop for the coolant of 20 Ah lithium-ion pouch cell with varying the number of channels and the mass flow rates. The number of channels is varied from 4 to 10 and the mass flow rate is varied from 0.000833 kg/s to 0.003333 kg/s. The pressure drop is directly indicative of pumping cost, and must be kept as low as possible. As shown in Figure 7, the number of channels and the mass flow rates have the opposite influence on the pressure drop. As a result, to provide better energy efficiency, the number of channels and the mass flow rates could be optimized. The pressure drop increased by 466.8% as the number of channels decreased from 10 to 4. The pressure drop increased by 1124.0% as the mass flow rate of the coolant is increased from 0.000833 kg/s to 0.003333 kg/s. The effect of both parameters of the mass flow rate as well as the number of channels on the pressure drop are significant.
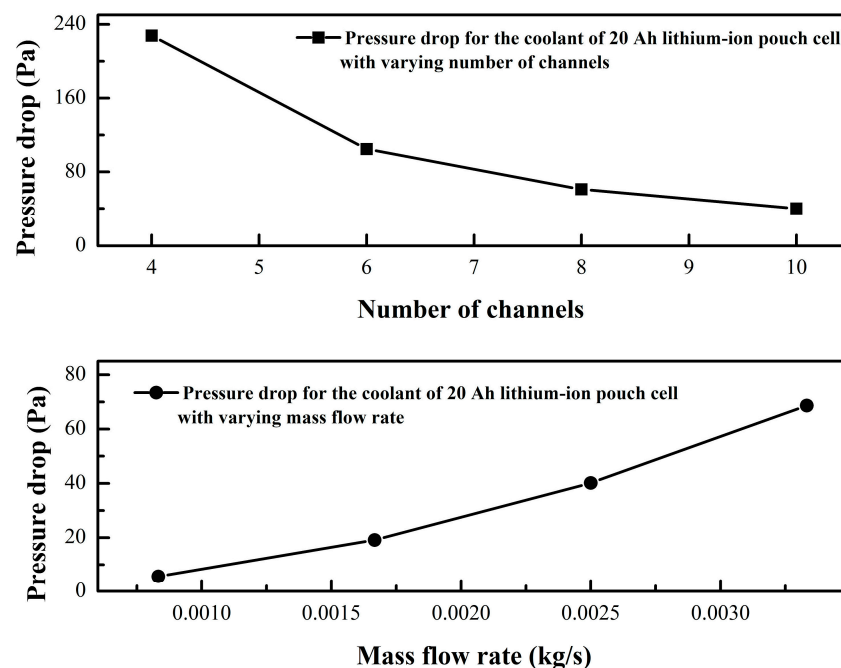

Figure 7. Pressure drop for the coolant of 20 Ah lithium-ion pouch cell with varying the number of channels and the mass flow rate.

3.4. Cooling Energy Efficiency

Figure 8 shows the cooling energy efficiency (β) of the 20 Ah lithium-ion pouch cell with a surface area coverage ratio (α) parameter of 0.750. Figure 8a,b show the cooling energy efficiency parameter (β) of the 20 Ah lithium-ion pouch cell for 1C and 2C discharge rates, respectively. For both 1C and 2C discharge rates, the cooling energy efficiency parameter (β) decreased with the increase of the inlet coolant mass flow rate varying from 0.000833 kg/s to 0.003333 kg/s for surface area coverage

ratio (α) parameter of 0.750. For the low inlet coolant mass flow rate, the energy efficiency parameter significantly increased with the decrease of an inlet coolant temperature. However, for the high inlet coolant mass flow rate, the energy efficiency parameters are changed slightly with the increase of the inlet coolant temperature. This indicates that, for both 1C and 2C discharge rates, for the low inlet coolant mass flow rate, the lower inlet coolant temperature provides the better energy efficiency in the 20 Ah lithium-ion pouch cell with cold plates along both surfaces. As shown in the Figure 8a,b, with inlet coolant mass flow rates varying from 0.001667 kg/s to 0.003333 kg/s, the reduction scale of the energy efficiency parameter is lower than those of the inlet coolant mass flow rates varying from 0.000833 kg/s to 0.001667 kg/s for the different inlet coolant temperatures. Comparing with Figure 8a and Figure 8b, the energy efficiency parameters are close for 1C discharge rate for the inlet coolant temperatures of 5 °C and 15 °C, respectively, for the inlet mass flow rate coolant varying from 0.000833 kg/s to 0.001667 kg/s.
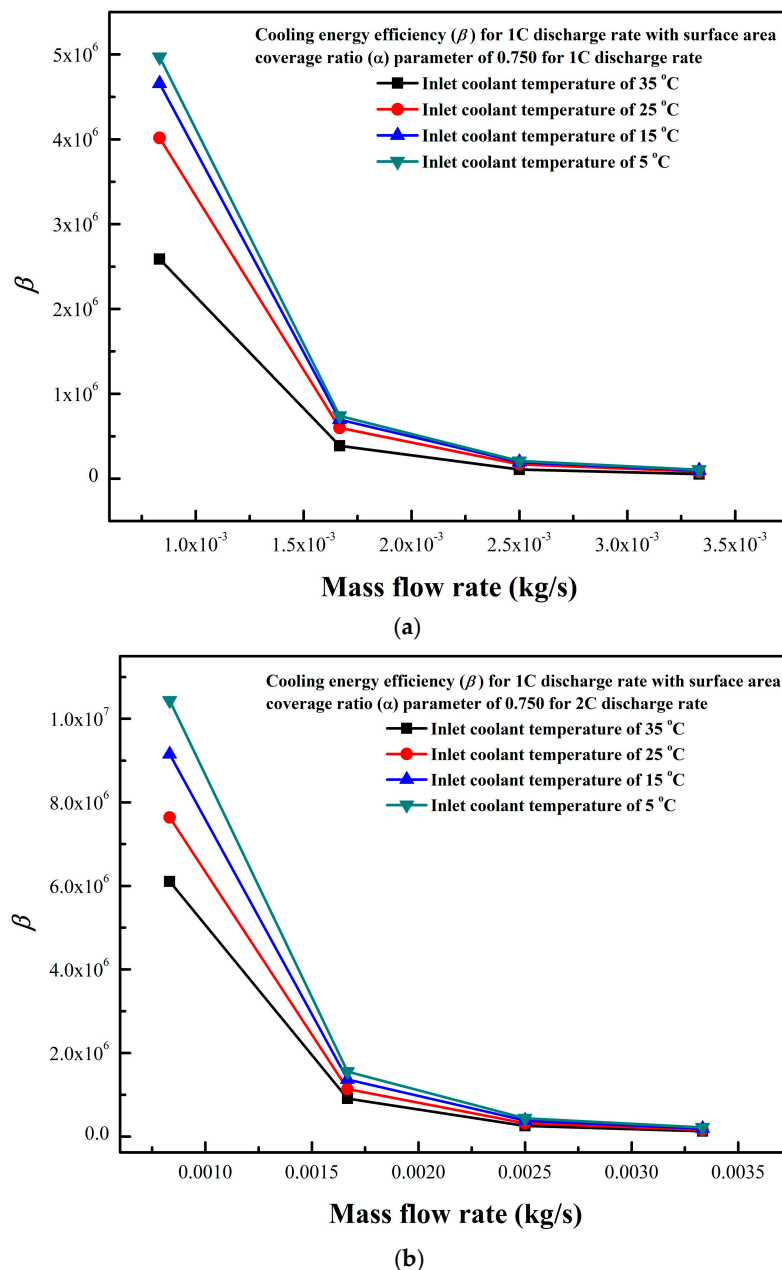

(a)

(b)

Figure 8. Cooling energy efficiency (β) of 20 Ah lithium-ion pouch cell with surface area coverage ratio (α) parameter of 0.750: (**a**) 1C; (**b**) 2C.

As shown in the Figure 8a, the lowest energy efficiency parameter (β) is above 54,000 for the inlet coolant temperature of 35 °C and the inlet coolant mass flow rate of 0.003333 kg/s. This value is significant based on the definition of an energy efficiency parameter [25]. Therefore, it can be concluded that for the inlet coolant temperature of 5 °C and the inlet coolant mass flow rate of 0.000833 kg/s, the 20 Ah lithium-ion pouch cell with cold plates on both sides shows excellent cooling effectiveness. This is because of more heat removal capacity of the lower inlet coolant temperature and the lower power consumption for supplying coolant at low mass flow rate.

Figure 9 shows the cooling energy efficiency (β) of the 20 Ah lithium-ion pouch cell with the inlet coolant mass flow rate of 0.025 kg/s. Figure 9a,b show the cooling energy efficiency parameters (β) of the 20 Ah lithium-ion pouch cell for 1C and 2C discharge rates, respectively. The cooling energy efficiency parameter (β) increased with increase of the surface area coverage ratio (α) parameter from 0.298 to 0.750 for the inlet coolant mass flow rate of 0.002500 kg/s. For the higher surface area coverage ratio (α) parameter, the cooling energy efficiency parameter (β) significantly increased with the decrease of an inlet coolant temperature. However, for the lower surface area coverage ratio (α) parameter, the cooling energy efficiency parameter (β) is changed slightly with the decrease of an inlet coolant temperature. This indicates that for the low inlet coolant temperature, the higher surface area coverage ratio (α) parameter provided the better energy efficiency for the 20 Ah lithium-ion pouch cell with cold plates along both surfaces. As shown in Figure 9a,b, with the surface area coverage ratio (α) parameter varying from 0.599 to 0.750, the enhancement scale of the energy efficiency parameter is higher than that of surface area coverage ratio (α) parameter varying from 0.298 to 0.599 for the different inlet coolant temperatures. Comparing with Figure 9a and Figure 9b, the cooling energy efficiency parameter (β) is close for 1C discharge rate for the inlet coolant temperatures of 5 °C and 15 °C, respectively, for the surface area coverage ratio (α) parameter varying from 0.298 to 0.750. As shown in the Figure 9a, the lowest cooling energy efficiency parameter (β) is above 43900 for the surface area coverage ratio (α) parameter of 0.298 and the inlet coolant temperature of 35 °C. This value is significant based on the definition of an energy efficiency parameter [25]. Therefore, it can be concluded that for the inlet coolant temperature of 5 °C and the surface area coverage ratio (α) parameter of 0.750, the 20 Ah lithium-ion pouch cell with cold plates on both sides shows an excellent cooling effectiveness because of heat removal capacity of the lower inlet coolant temperature and lower power consumption for supplying the coolant at high surface area coverage ratio (α) parameter.

In addition, the low inlet coolant temperature, the low inlet coolant mass flow rate, and high number of the cooling channels showed excellent cooling energy efficiency. The effects of the inlet coolant temperatures, the inlet coolant mass flow rates, and the surface area coverage ratio (α) parameter on three key parameters, namely, maximum temperature, temperature non-uniformity and cooling energy efficiency, are reported, and will be helpful to optimize the cooling strategy for lithium-ion pouch cell with cold plates on both surfaces.
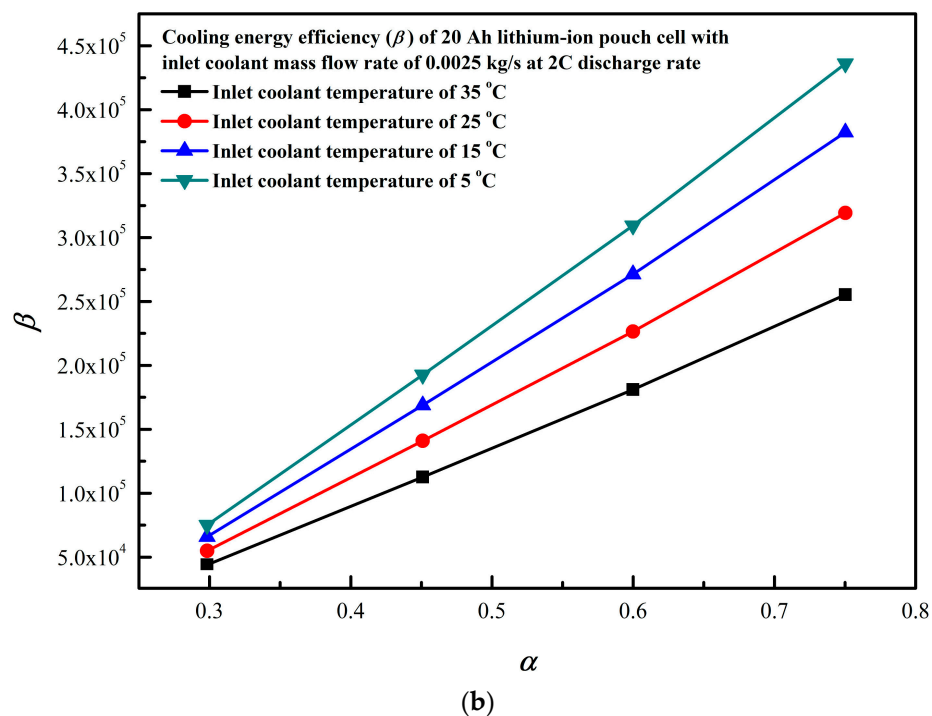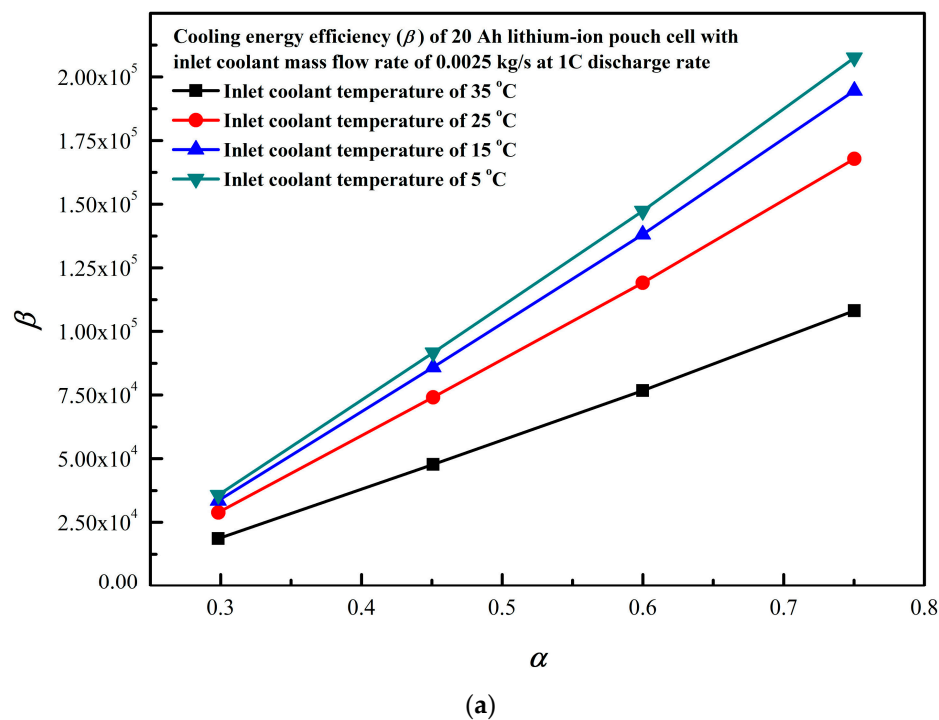
(**a**)

(**b**)

Figure 9. Cooling energy efficiency (*β*) of 20 Ah lithium-ion pouch cell with inlet coolant mass flow rate of 0.025 kg/s: (**a**) 1C; (**b**) 2C.

3.5. Flow Visualization

Figure 10 shows the velocity distribution of the 20 Ah lithium-ion pouch cell cooling system for the different number of the channels. The uniform velocity distribution is observed throughout, except at curved flow paths with relatively higher velocity gradients. The velocity contours are obtained at the mid-plane of the cooling plate. For the channel number 4, a maximum velocity of 0.190 m/s is observed, while for the channel number 10, the maximum velocity of 0.077 m/s is observed. The general flow patterns are similar with the high velocity flow for lower number of the channels.
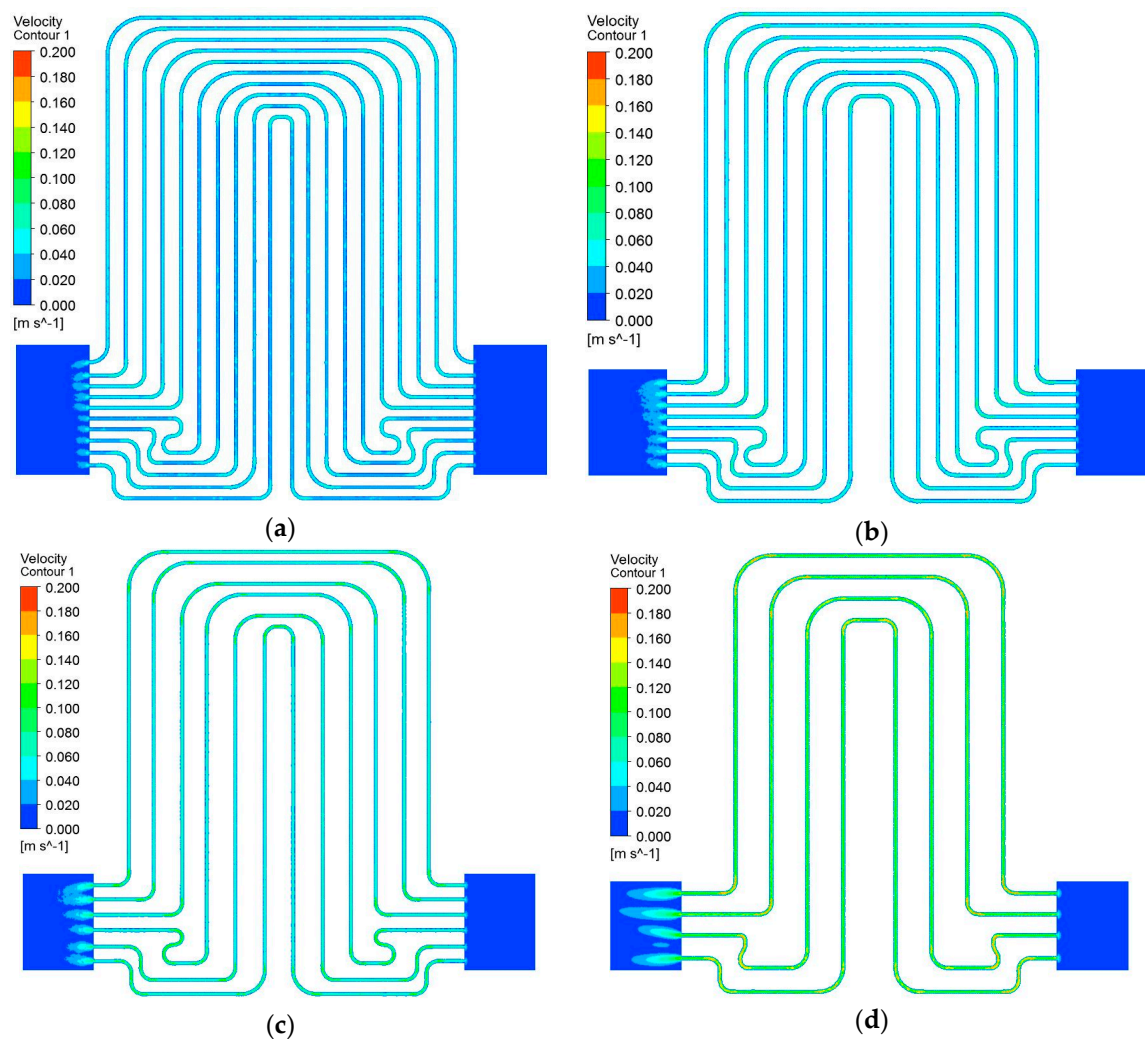
Figure 10. Velocity distribution of 20 Ah lithium-ion pouch cell cooling system for different numbers of channels: (**a**) 10; (**b**) 8; (**c**); 6 (**d**) 4.

4. Conclusions

The cooling performance characteristics of a 20 Ah lithium-ion pouch cell with cold plates along both surfaces are studied numerically. The effects of variation of the inlet coolant mass flow rates (0.000833 kg/s, 0.001667 kg/s, 0.002500 kg/s, 0.003333 kg/s) and the inlet coolant temperatures (5 °C, 15 °C, 25 °C, 35 °C) for 1C and 2C discharge rates are reported. The temperature distribution, the pressure drop, and the cooling energy efficiency are considered as the critical performance parameters. In addition, the effects of the variation in the cold plate geometry with the number of the channels (4, 6, 8, 10) on the cooling performance characteristics of 20 Ah lithium-ion pouch cell are reported. The maximum temperature of 20 Ah lithium-ion pouch cell obtained at 2C discharge rate is 45.2 °C for the inlet coolant temperature of 35 °C and the inlet coolant mass flow rate of 0.000833 kg/s. The key results are provided below:

- Considering the maximum temperature, for providing optimum operating temperature in the range of 25 °C to 40 °C for 20 Ah lithium-ion pouch cell for 1C and 2C discharge rate with cold plates along both surfaces, the inlet coolant temperatures of 15 °C and 25 °C are suggested.
- Considering the difference between the maximum and the minimum temperature, for providing optimum operating difference between the maximum and the minimum temperatures below 5 °C for 20 Ah lithium-ion pouch cell for 1C and 2C discharge rate with cold plates along both surfaces, the inlet coolant mass flow rates of 0.002500 kg/s and 0.003333 kg/s are suggested.

- The highest pressure drop of the coolant of 20 Ah lithium-ion pouch cell is 227.6 Pa for the mass flow rate of 0.001667 kg/s with 4 number of the channels.
- Considering the cooling energy efficiency (β) of 20 Ah lithium-ion pouch cell with a surface area coverage ratio (α) parameter of 0.750, for the inlet coolant temperature of 5 °C and the inlet coolant mass flow rates of 0.000833 kg/s, the lithium-ion pouch cell with cold plates on both sides shows an excellent cooling effectiveness.
- Considering the cooling energy efficiency (β) of 20 Ah lithium-ion pouch cell with the inlet coolant mass flow rate of 0.025 kg/s, an inlet coolant temperature of 5 °C and the surface area coverage ratio (α) parameter of 0.750, the lithium-ion pouch cell with cold plates on both sides shows an excellent cooling effectiveness.

The effects of inlet coolant temperature, inlet coolant mass flow rate, the surface area coverage ratio on three key parameters, namely, maximum temperature, temperature uniformity, and cooling energy efficiency of 20 Ah lithium-ion pouch cell with cold plates along both surfaces are reported, and will be useful for optimizing the cooling performances in the applications of the thermal management systems of the lithium-ion batteries for the electric vehicles.

Nomenclature

C_1	model constants
C_2	model constants
C_3	model constants
C_p	Specific heat at constant pressure (J/kg·°C)
C_μ	constant
G_k	generation of turbulence kinetic energy due to the mean velocity gradients
G_b	generation of turbulence kinetic energy due to buoyancy
k	turbulent kinetic energy (J)
m	mass flow rate
P	pressure (Pa)
Pr	Prandtl number
Q	heat transfer rate (W)
Qv	volumetric flow rate (m^3/s)
S_k	user-defined source terms
S_ε	user-defined source terms
T	temperature (°C)
ΔT	temperature difference (°C)
t	time (s)
V	speed (m/s)
$\overline{V}$	average velocity (m/s)
v_s	mean fluid velocity (m/s)
Y_M	the contribution of the fluctuating dilatation in compressible turbulence to the overall dissipation rate

Greek symbols

∇	gradient operator
β	cooling energy efficiency
ρ	density (kg/m^3)
ν	kinematic fluid viscosity (m^2/s)

μ dynamic fluid viscosity (Ns/m^2)

λ Reynold's stress

σ_k turbulent Prandtl numbers for k

ε_k turbulent Prandtl numbers for ε

Acronyms

C   current discharge rate

CAD   computer-aided design

CFD   computational fluid dynamics

EV   electric vehicle

HEV   hybrid electric vehicles

PCM   phase change material

References

1. Campanari, S.; Manzolini, G.; Iglesia, F.G.D.I. Energy analysis of electric vehicles using batteries or fuel cells through well-to-wheel driving cycle simulations. *J. Power Sources* **2009**, *186*, 464–477. [CrossRef]

2. Cicconi, P.P.; Landi, D.; Germani, M. Thermal analysis and simulation of a Li-ion battery pack for a lightweight com-mercial EV. *Appl. Energy* **2017**, *192*, 159–177. [CrossRef]

3. Tong, W.; Koh, Q.; Birgersson, E.; Mujumdar, A.S.; Yap, C. Correlating uncertainties of a lithium-ion battery—A Monte Carlo simulation. *Int. J. Energy Res.* **2015**, *39*, 778–788. [CrossRef]

4. Seo, J.H.; Patil, M.S.; Cho, C.P.; Lee, M.Y. Heat transfer characteristics of the integrated heating system for cabin and battery of an electric vehicle under cold weather conditions. *Int. J. Heat Mass Transf.* **2018**, *117*, 80–94. [CrossRef]

5. Zubi, G.; López, R.D.; Carvalho, M.; Pasaoglu, G. The lithium-ion battery: State of the art and future perspectives. *Renew. Sustain. Energy Rev.* **2018**, *89*, 292–308. [CrossRef]

6. Pesaran, A.A. Battery thermal models for hybrid vehicle simulations. *J. Power Sources* **2002**, *110*, 377–382. [CrossRef]

7. Coman, P.T.; Darcy, C.E.; Veje, C.T.; White, R.E. Numerical analysis of heat propagation in a battery pack using a novel technology for triggering thermal runaway. *Appl. Energy* **2017**, *203*, 189–200. [CrossRef]

8. Kvasha, A.; Gutiérrez, C.; Osa, U.; Meatza, I.D.; Blazquez, J.A.; Macicior, H.; Urdampilleta, I. A comparative study of thermal runaway of commercial lithium ion cells. *Energy* **2018**, *159*, 547–557. [CrossRef]

9. Feng, X.; Ouyang, M.; Liu, X.; Lu, L.; Xia, Y.; He, X. Thermal runaway mechanism of lithium ion battery for electric vehicles: A review. *Energy Storage Mater.* **2018**, *10*, 246–267. [CrossRef]

10. Deng, Y.; Feng, C.; Zhu, J.E.H.; Chen, J.; Wen, M.; Yin, H. Effects of different coolants and cooling strategies on the cooling performance of the power lithium ion battery system: A review. *Appl. Therm. Eng.* **2018**, *142*, 10–29. [CrossRef]

11. Saw, L.H.; Ye, Y.; Tay, A.A.O.; Chong, W.T.; Kuan, S.H.; Yew, M.C. Computational fluid dynamic and thermal analysis of Lithium-ion battery pack with air cooling. *Appl. Energy* **2016**, *177*, 783–792. [CrossRef]

12. Ling, Z.; Cao, J.; Zhang, W.; Zhang, Z.; Fang, X.; Gao, X. Compact liquid cooling strategy with phase change materials for Li-ion batteries optimized using response surface methodology. *Appl. Energy* **2018**, *228*, 777–788. [CrossRef]

13. Ianniciello, L.; Biwolé, P.H.; Achard, P. Electric vehicles batteries thermal management systems employing phase change materials. *J. Power Sources* **2018**, *378*, 383–403. [CrossRef]

14. Patil, M.S.; Seo, J.H.; Bang, Y.M.; Kim, D.W.; Ekanayake, G.; Kim, H.M.; Choi, Y.H.; Lee, M.Y. A Novel Design for Lithium ion Battery cooling using Mineral Oil. In Proceedings of the 3rd International Mega-Conference on Green and Smart Technology (GST 2016), Jeju National University, Jeju island, Korea, 21–23 December 2016; Volume 141, pp. 164–168.

15. Seo, J.H.; Patil, M.S.; Kim, D.W.; Bang, Y.M.; Lee, M.Y. Numerical Study on the Cooling Performances of Various Cooling Methods for Laminated Type Battery. In Proceedings of the 1st ACTS—Asian Conference on Thermal Sciences 2017, Jeju Island, Korea, 26–30 March 2017.

16. Panchal, S.; Khasow, R.; Dincer, I.; Agelin-Chaab, M.; Fraser, R.; Fowler, M. Thermal design and simulation of mini-channel cold plate for water cooled large sized prismatic lith-ium-ion battery. *Appl. Therm. Eng.* **2017**, *122*, 80–90. [CrossRef]

17. Shen, X.; Liu, H.; Cheng, X.B.; Yan, C.; Huang, J.Q. Beyond lithium ion batteries: Higher energy density battery systems based on lithium metal anodes. *Energy Storage Mater.* **2018**, *12*, 161–175. [CrossRef]

18. Panchal, S.; Khasow, R.; Dincer, I.; Agelin-Chaab, M.; Fraser, R.; Fowler, M. Numerical modeling and experimental investigation of a prismatic battery subjected to water cooling. *Numer. Heat Transf. Part A Appl.* **2017**, *71*, 626–637. [CrossRef]

19. Panchal, S.; Dincer, I.; Agelin-Chaab, M.; Fraser, R.; Fowler, M. Thermal modeling and validation of temperature distributions in a prismatic lithium-ion battery at different discharge rates and varying boundary conditions. *Appl. Therm. Eng.* **2016**, *96*, 190–199. [CrossRef]

20. Panchal, S.; Mathewson, S.; Fraser, R.; Culham, R.; Fowler, M. Thermal Management of Lithium-Ion Pouch Cell with Indirect Liquid Cooling using Dual Cold Plates Approach. *SAE Int. J. Altern. Power-Trains* **2015**, *4*, 293–307. [CrossRef]

21. *ANSYS® Academic Research, Release 18.0*, ANSYS Inc.: Canonsburg, PA, USA, 2017.

22. Chen, D.; Jiang, J.; Kim, G.H.; Yang, C.; Pesaran, A. Com-parison of different cooling methods for lithium ion battery cells. *Appl. Therm. Eng.* **2016**, *94*, 846–854. [CrossRef]

23. Qian, Z.; Li, Y.; Rao, Z. Thermal performance of lithium-ion battery thermal management system by using mini-channel cooling. *Energy Convers. Manag.* **2016**, *126*, 622–631. [CrossRef]

24. Song, W.; Chen, M.; Bai, F.; Lin, S.; Chen, Y.; Feng, Z. Non-uniform effect on the thermal/aging performance of Lithium-ion pouch battery. *Appl. Therm. Eng.* **2018**, *128*, 1165–1174. [CrossRef]

25. Lu, Z.; Yu, X.; Wei, L.; Qiu, Y.; Zhang, L.; Meng, X.; Jin, L. Parametric study of forced air cooling strategy for lithium-ion battery pack with staggered arrangement. *Appl. Therm. Eng.* **2018**, *136*, 28–40. [CrossRef]